Progress In Electromagnetics Research, PIER 72, 105–126, 2007

FAST MULTIPOLE ACCELERATED SCATTERING MATRIX METHOD FOR MULTIPLE SCATTERING OF A LARGE NUMBER OF CYLINDERS

Y. J. Zhang

EMC Laboratory
Department of Electrical & Computer Engineering
209 Emerson Electric Company Hall
University of Missouri-Rolla
Rolla, MO 65409, USA

E. P. Li

Engineering Software
Institute of High Performance Computing
#01-01 Capricorn, 1 Science Park Rd., 117528, Singapore

Abstract—The lowering and raising operators of cylindrical harmonics are used to derive the general fast multipole expressions of arbitrary order Hankel functions. These expressions are then employed to transform the dense matrix in the scattering matrix method (SMM) into a combination of sparse matrices (aggregation, translation and disaggregation matrices). The novel method is referred to as fast multipole accelerated scattering matrix method (FMA-SMM). Theoretical study shows FMA-SMM has lower complexity $O(N^{1.5})$ instead of SMM's $O(N^2)$, where N stands for total harmonics number used. An empirical formula is derived to relate the minimum group size in FMA-SMM to the highest order Hankel functions involved. The various implementation parameters are carefully investigated to guarantee the algorithm's accuracy and efficiency. The impact of the cylinders density on convergence rate of iterative solvers (BiCGStab(2) here), memory cost as well as CPU time is also investigated. Up to thousands of cylinders can be easily simulated and potential applications in photonic crystal devices are illustrated.

1. INTRODUCTION

Scattering matrix method, also called T-matrix method or Foldy-Lax equations, is usually used to calculate the multiple scattering of many objects, the cases usually encountered in remote sensing modelling. The original theory was first proposed by Foldy [1], then developed by Lax [2] and many other authors [3–6]. The T-matrix of a single object relates the scattered waves to the incident waves in its local coordinates, based on the expansions of cylindrical harmonics in two-dimensional (2D) cases as well as spherical harmonics in three-dimensional (3D) cases. This description has the benefit of independence to the directions or angles of incident waves. Thus, with the aid of the addition theorems of cylindrical or spherical harmonics, T-matrix method allows straightforward consideration of the multiple scattering effects of many objects. However, just like the traditional method of moments (MoM), traditional T-matrix method has the computational complexity of $O(N^2)$ where N is the total harmonics number used for all objects.

To explore fast algorithms based on T-matrix method, Chew et al. have proposed several kinds of recursive aggregated T-matrix algorithms (RATMA) for either 2D or 3D scattering problems [7]. In these algorithms, an arbitrary shaped target is first meshed into many small elements represented by circular cylinders or spheres whose T-matrix can be derived analytically. These elements are naturally located layer-by-layer from the center point of the target. Then the addition theorems of harmonics are recursively used to derive the aggregated T-matrix from inner layer to outer layer, and finally the T-matrix of the whole target can be obtained. The advantage of such kind of algorithms is that the monostatic scattering is easily calculated once the T-matrix of the target has been derived. However, the complexity of RATMA remains $O(N^2)$, which prohibits its further applications in large problems.

Recently, scattering matrix method has found many new applications such as the analysis of finite size photonic crystal devices [8–10] and metamaterials [11, 12]. Moreover, the authors of [13] proposed an innovative way to apply this method to 3D photonic crystal structures. A similar method, generalized multipole technique, is recently used to analyze a lossy microring add-drop optical filter in [14]. Unlike mesh based numerical methods such as finite difference time domain (FDTD) and finite element method (FEM), T-matrix method takes advantage of the specific structure of photonic crystals and uses cylindrical harmonics to express the field distributions. Although this semi-analytical approach is found to be nearly ten times

faster than FDTD or FEM [9], it is still cumbersome to be used for the design of large photonic crystal structures due to its relatively higher computational complexity.

The objective of this paper is to develop an efficient scattering matrix method accelerated by fast multipole method for multiple scattering of a large number of cylinders. It is worth noting that some efforts have been put on fast multipole method (FMM) in 3D multiple scattering problems for Helmholtz equation. (More details can be obtained by referring to [15–17] and the book written by N. A. Gumerov and R. Duraiswami [18]). However, to the best of our knowledge, there is no description of utilizing FMM into 2D scattering matrix method so far.

FMM has been extensively used in solving integral equations arising from electromagnetic scattering [19–22]. The principal formula in 2D FMM is to express the far field of the Green's function into an integration involving the diagonalized translation operator, see Eq. (13) in [21]. In the 2D case, to facilitate our description, we call it the fast multipole expression of the zero-order Hankel function. Obviously, the previous FMM can not be used directly in the scattering matrix method since the higher-order, instead of only the zero-order, Hankel functions are often required to express the field distribution of each cylinder. To extend the applications of FMM in scattering matrix method, we first derived the general fast multipole expressions of arbitrary order Hankel functions by using the lowering and raising operators of the cylindrical harmonics. Then, these general expressions are employed to convert the dense matrix in scattering matrix method into a combination of sparse matrices. Similar to the conventional FMM, these sparse matrices can be named as aggregation matrix, translation matrix and disaggregation matrix. Theoretical investigation shows that the computational complexity of the fast multipole accelerated scattering matrix method (FMA-SMM) is $O(N^{1.5})$.

This paper is organized as follows. Section 2 briefly introduces the scattering matrix method. In Section 3, the general fast multipole expressions of arbitrary order Hankel functions are derived. To facilitate the implementation of the algorithm, the sparse matrix form of the FMA-SMM is provided. The implementation rules, which are different from conventional FMM, for various parameters of the algorithm are presented in Section 4 to ensure the accuracy of the algorithm. Validation and some numerical examples are provided in Section 5 followed by a short summary of this work.

2. SCATTERING MATRIX METHOD

Consider a set of randomly distributed cylindrical rods shown in Fig. 1, where the rods can be different in radii and dielectric constants. For an observation point $\vec{\rho}$ outside of all the rods, the scattered field can be expressed as the summation of all the scattered waves from each rod, and given by

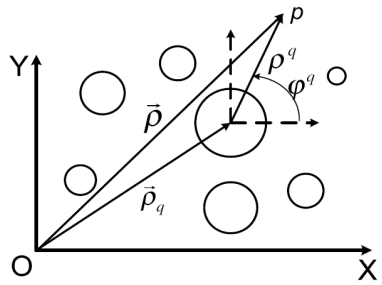

Figure 1. Schematic of a set of random cylindrical rods.

$$\Phi(\vec{\rho}) = \sum_{q=1}^{N_c} \sum_{n=-M_q}^{M_q} f_q^n H_n^{(2)}(k\rho^q) e^{jn\phi^q} \tag{1}$$

where symbols (ρ^q, ϕ^q) is the local coordinates defined as $\rho^q = |\vec{\rho} - \vec{\rho}_q|$, $\phi^q = arg\{\vec{\rho} - \vec{\rho}_q\}$; N_c is the total number of rods and $2M_q+1$ represents the truncated number of Hankel functions used to express the scattered waves of qth rod and f_q^n is the corresponding unknown expansion coefficients $(n = -M_q, -M_q + 1, \cdots, M_q)$. The unknown expansion coefficients vector $\mathbf{f}_q$ satisfies the following equation:

$$\mathbf{f}_q = \mathbf{T}_q \left(\mathbf{a}_q + \sum_{p=1; p\neq q}^{N_c} \mathbf{A}_{qp} \mathbf{f}_p \right) \tag{2}$$

where $\mathbf{T}_q$ stands for the T-matrix of qth rod; $\mathbf{a}_q$ denotes the expansion coefficients of incident wave on qth rod in terms of Bessel functions. Matrix $\mathbf{A}_{qp}$ represents the translation matrix between the pth and the qth rods, representing the incident wave of qth rod caused by the scattered wave of pth rod. The elements of the translation matrix can be derived from the following addition theorem of cylindrical harmonics

(Appendix D, [23])

$$H_n^{(2)}(k\rho^p)e^{jn\phi^p} = \sum_{m=-\infty}^{\infty} \left[H_{m-n}^{(2)}(k\rho_{pq})e^{-j(m-n)\phi_{pq}}\right] J_m(k\rho^q)e^{jm\phi^q} \quad (3)$$

where symbols ρ_{pq} and ϕ_{pq} are defined as $\rho_{pq} = |\vec{\rho}_p - \vec{\rho}_q|, \phi_{pq} = arg\{\vec{\rho}_p - \vec{\rho}_q\}$. Therefore, matrix $\mathbf{A}_{qp}$ can be obtained by

$$\mathbf{A}_{qp}(m,n) = H_{m-n}^{(2)}(k\rho_{pq})e^{-j(m-n)\phi_{pq}} \quad (4)$$

Collecting (2) for all the rods yields a linear system of equations

$$(\mathbf{I} - \mathbf{TS})\mathbf{f} = \mathbf{Ta} \quad (5)$$

where $\mathbf{I}$ is the unit matrix; $\mathbf{T}$ is the block diagonal matrix expressed as $\mathbf{T} = diag\{\mathbf{T}_1, \mathbf{T}_2, \cdots, \mathbf{T}_{N_c}\}$; vector $\mathbf{f} = [\mathbf{f}_1, \mathbf{f}_2, \cdots, \mathbf{f}_{N_c}]^T$ stands for the unknown expansions of scattered waves and vector $\mathbf{a} = [\mathbf{a}_1, \mathbf{a}_2, \cdots, \mathbf{a}_{N_c}]^T$ is the expansion vector of incident waves on all the rods. Matrix $\mathbf{S}$ is the combined translation matrix written as

$$\mathbf{S} = \begin{bmatrix} \mathbf{0} & \mathbf{A}_{12} & \cdots & \mathbf{A}_{1N_c} \\ \mathbf{A}_{21} & \mathbf{0} & \cdots & \mathbf{A}_{2N_c} \\ \vdots & \vdots & \ddots & \vdots \\ \mathbf{A}_{N_c1} & \mathbf{A}_{N_c2} & \cdots & \mathbf{0} \end{bmatrix} \quad (6)$$

From (4), matrix $\mathbf{S}$ is a nearly full matrix whose storage is in the order of N^2, where $N = \sum_{p=1}^{N_c}(2M_p + 1)$ is the dimension of matrices and vectors in (5). Therefore, the computational complexity is $O(N^2)$ when an iterative solver is employed to get the solution of (5).

3. FAST MULTIPOLE ACCELERATED SCATTERING MATRIX METHOD

3.1. General Fast Multipole Expressions of Any Order Hankel Functions

To reduce the complexity of (5), the general fast multipole expressions of arbitrary order Hankel functions are first derived by using the following raising operator of Hankel functions (Eq. (2.2.16), [23]):

$$H_n^{(2)}(k\rho)e^{jn\phi} = -k^{-1}\left(\partial_x + j\partial_y\right) H_{n-1}^{(2)}(k\rho)e^{j(n-1)\phi} \quad (7)$$

and lowering operator

$$H_n^{(2)}(k\rho)e^{jn\phi} = k^{-1}\left(\partial_x - j\partial_y\right) H_{n+1}^{(2)}(k\rho)e^{j(n+1)\phi} \quad (8)$$

Since $H_{-n}^{(2)}(k\rho) = (-1)^n H_n^{(2)}(k\rho)$, we can rewrite (7) and (8) as

$$H_n^{(2)}(k\rho)e^{-jn\phi} = (-k)^{-n}\left(\partial_x - j\partial_y\right)^n H_0^{(2)}(k\rho) \quad (9)$$

$$H_{-n}^{(2)}(k\rho)e^{jn\phi} = k^{-n}\left(\partial_x + j\partial_y\right)^n H_0^{(2)}(k\rho) \quad (10)$$

for any $n \geq 0$. The fast multipole expression of the zero-order Hankel function has been given as [21]:

$$H_0^{(2)}(k\rho_{pq}) \simeq \frac{1}{2\pi}\int_0^{2\pi} \tilde{\beta}_{ps}(\alpha)T_{st}^P(\alpha)\tilde{\beta}_{qt}^*(\alpha)d\alpha \quad (11)$$

where symbol * stands for complex conjugate and function $T_{st}^P(\alpha)$ and $\tilde{\beta}_{ps}$ are defined as

$$T_{st}^P(\alpha) = \sum_{r=-P}^{P} H_r^{(2)}(k\rho_{st})e^{-jr(\phi_{st}-\alpha-\pi/2)} \quad (12)$$

$$\tilde{\beta}_{ps}(\alpha) = e^{jk(x_{ps}\cos\alpha + y_{ps}\sin\alpha)} \quad (13)$$

where $\rho_{st} = |\vec{\rho}_s - \vec{\rho}_t|$ and, $\vec{\rho}_s$ and $\vec{\rho}_t$ are the center of group g_s and g_t respectively, as shown in Fig. 2. (x_p, y_p) and (x_s, y_s) are the Cartesian coordinates of p-th rod and group g_s, respectively; and $x_{ps} = x_p - x_s, y_{ps} = y_p - y_s$.

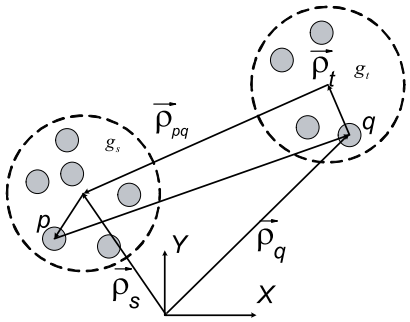

Figure 2. Geometry of groups and cylinders.

Substituting (11) into (9) and exchanging the integral and differential operators leads to the following equation after some mathematical treatments

$$H_n^{(2)}(k\rho_{pq})e^{-jn\phi_{pq}} \simeq \frac{1}{2\pi}\int_0^{2\pi} \tilde{\beta}_{ps}(\alpha)T_{st}^P(\alpha)\tilde{\beta}_{qt}^*(\alpha)e^{-jn(\alpha+\pi/2)}d\alpha \quad (14)$$

Similarly, substituting (11) into (10), we can obtain the same expression as (14). In other words, (14) is valid for arbitrary integer n, and can be viewed as the generalization of the conventional FMM expression of the zero-order Hankel function.

3.2. Sparse Matrix form of FMA-SMM

Replacing index n with $m-n$ in (14), the element of matrix $\mathbf{A}_{qp}$ given in (4) can be rewritten as

$$\mathbf{A}_{qp}(m,n) \simeq \frac{1}{2\pi}\int_0^{2\pi} \tilde{\beta}_{ps}(n,\alpha) T_{st}^P(\alpha) \tilde{\beta}_{qt}^*(m,\alpha) d\alpha \tag{15}$$

$$\tilde{\beta}_{ps}(n,\alpha) = e^{jk(x_{ps}\cos\alpha + y_{ps}\sin\alpha) + jn(\alpha+\pi/2)} \tag{16}$$

$$\tilde{\beta}_{qt}(m,\alpha) = e^{jk(x_{qt}\cos\alpha + y_{qt}\sin\alpha) + jm(\alpha+\pi/2)} \tag{17}$$

We select Q sampling points of the polar angle α to approximate the integration of (15) as

$$\mathbf{A}_{qp}^F(m,n) \simeq \frac{1}{Q}\sum_{r=0}^{Q} \tilde{\beta}_{ps}(n,\alpha_r) T_{st}^P(\alpha_r) \tilde{\beta}_{qt}^*(m,\alpha_r) \tag{18}$$

where the sampling angle $\alpha_r = 2\pi r/(Q-1)$. Here, we use symbol $\mathbf{A}_{qp}^F(m,n)$ to differentiate the approximation expression of (18) from the exact $\mathbf{A}_{qp}(m,n)$ of (4).

In the procedure of fast multipole method, all rods are distributed into groups according to the distance to the group centers. To each group, all groups can be classified into a near group set and a far group set. For example, to group g_t, we denote its near group set as Ng_t and far group set as Fg_t. We assume that p-th and q-th rod belongs to group g_s and g_t respectively. If g_s belongs to the near group set Ng_t, exact formula (4) is used to calculate the interaction of rods p and q. On the other hand, if g_s belongs to the far group set Fg_t, the approximation expression (18) would be adopted instead. Therefore, (2) is converted into

$$\mathbf{f}_q = \mathbf{T}_q \left(\mathbf{a}_q + \sum_{p\in g_s; g_s \in Ng_t} \mathbf{A}_{qp}\mathbf{f}_p + \sum_{p\in g_s; g_s \in Fg_t} \mathbf{A}_{qp}^F \mathbf{f}_p \right) \tag{19}$$

where the $(2M_q+1)\times(2M_p+1)$ matrix $\mathbf{A}_{qp}^F$ can be decomposed from (18) as

$$\mathbf{A}_{qp}^F = \frac{1}{Q}\mathbf{V}_q^+ \mathbf{M}_{qp} \mathbf{V}_p \tag{20}$$

here the symbol '+' denotes the transpose conjugate matrix; $\mathbf{V}_p(\mathbf{V}_q)$ is a $Q \times (2M_{p(q)} + 1)$ matrix whose elements are

$$\mathbf{V}_{p(q)}(r, n) = \tilde{\beta}_{ps(qt)}(n, \alpha_r), \quad n \in [-M_{p(q)}, M_{p(q)}] \tag{21}$$

and $\mathbf{M}_{qp}$ is a $Q \times Q$ diagonal matrix whose elements are obtained by $T_{st}^P(\alpha_r), r = 1, 2, \cdots Q$.

Substituting (20) into (19) and combining the equations for all the rods, the final equation of fast multipole accelerated scattering matrix method is derived as

$$\left[\mathbf{I} - \mathbf{T}\left(\mathbf{S}_N + \frac{1}{Q}\mathbf{V}^+\mathbf{M}\mathbf{V}\right)\right]\mathbf{f} = \mathbf{T}\mathbf{a} \tag{22}$$

where $\mathbf{S}_N$ represents the near group interaction while the sparse matrix $\mathbf{V}$ is the aggregation matrix, and $\mathbf{M}$ denotes the translation matrix.

3.3. Complexity of the Fast Multipole Accelerated Scattering Matrix Method

When an iterative method, e.g., Bi-conjugate gradient Stabilized (BiCGStab) [24], is used to solve (22), the computational complexity of the matrix-vector product involved is in the same order as the storage of all sparse matrices. We assume that a total of N_c rods are distributed in G groups and an average of M cylindrical harmonics are used to model each rod. Furthermore, for each group, there are an average of p near groups. Then, the orders of non-zero elements in each sparse matrix are listed below

$$\mathbf{S}_N \sim p\frac{(N_c M)^2}{G} \tag{23}$$

$$\mathbf{V} \sim QN_cM \tag{24}$$

$$\mathbf{M} \sim G(G-p)Q \tag{25}$$

Similar to the discussion in [21], parameters G and Q are set into the same order of $\sqrt{N}$, i.e., $G \sim c_1\sqrt{N}$ and $Q \sim c_2\sqrt{N}$, where $N = N_cM$ is the total number of unknowns. Therefore, the total storage of non-zero elements of sparse matrices in (22) is in the order of $\left[p/c_1 + c_2 + (1 - \frac{p}{c_1\sqrt{N}})c_1c_2\right] N^{1.5}$ and c_1, c_2 are implementation constants. So the theoretical computational complexity of the FMA-SMM is $O(N^{1.5})$. This complexity can be further reduced by its multilevel version [22].

4. IMPLEMENTATION OF THE FMA-SMM

The implementation of the fast multipole method requires setting up of group structures. In traditional FMM for integral equations, the discretized elements are first enclosed in a squared box and the box is divided into four small equally sized boxes. This procedure is repeated until the dimension of the smallest box, or group, satisfies the requirement. The details of setting up hierarchical group structures can be found in [22]. For conventional fast multipole method, the dimension of the smallest group can be about half wavelength. However, great errors have been found if the minimum group size is set to be half wavelength for FMA-SMM implementation. Therefore, how to select various parameters, including the accuracy criterion, the group size, the multipole number P in (12) and the sampling point number Q in (18), becomes critical.

Rigorous study of the constraints among these parameters needs more careful mathematical analysis. Here, we adopt a numerical approach to provide an empirical rule for selection of these parameters.

From the exact expression (4) and its FMM approximation (18), a relative error $\triangle\varepsilon$ is defined as

$$\triangle\varepsilon(p, q, \rho_{st}, P, Q, m-n) = \frac{|\mathbf{A}_{qp}(m,n) - \mathbf{A}^F_{qp}(m,n)|}{|\mathbf{A}_{qp}(m,n)|} \tag{26}$$

Here $\triangle\varepsilon$ is a function of source point p, observation point q, expansion multipole number P, sampling points Q and the order of Hankel functions. We assume that a hierarchical group structure has been constructed. Fig. 3 shows a schematic of part of the group structure with source group s, target group t_1 and t_2, and the corresponding rods p and q.

If target group t_1 is the nearest far group of source group s, we call it 1 box buffer size implementation. This means that the near groups of group s are located on only one surrounding layer from it. On the other hand, if target group t_2 is the nearest far group of group s, it is called 2 box buffer size implementation. In this paper, we restrict ourselves to the discussion of 1 box buffer size implementation due to its easiness for the future implementation in its multilevel version.

It is very complicated to investigate the relative error versus so many parameters simultaneously. Fortunately, after extensive numerical tests, we found following properties for the various implementation parameters:

- For a specific order of Hankel function $m - n$, the relative error (26) becomes maximum when source point p and target point q are located at the corners of the groups shown in Fig. 3.

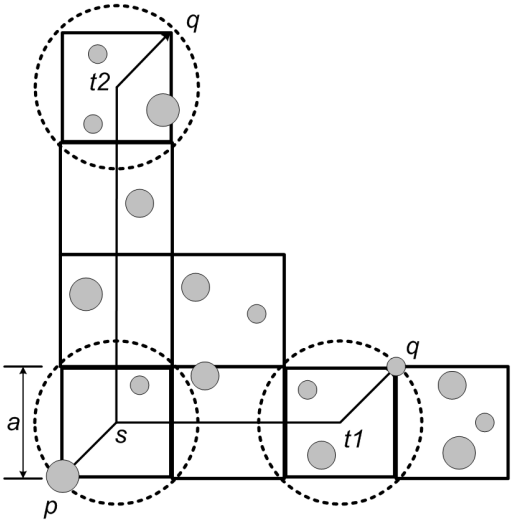

Figure 3. Schematic of a part of the group structure.

- For a specific multipole number P, the relative error $\triangle\varepsilon$ will decrease steadily with the increase of Q until $Q = 2P + 1$. The increase of Q after $2P+1$ would not reduce $\triangle\varepsilon$ significantly. Since the increase of the sampling point number Q will dramatically increase the storage cost, we strongly suggested $Q = 2P + 1$.
- The multipole number P can be selected as similar expression given in [25] as

$$2P + 1 = int\left(c_1 kD + c_2(kD)^{1/3}\right) \tag{27}$$

where $kD = \sqrt{2}ka$ is the diameter of groups and the function $int(x)$ is the greatest integer less than or equal to real number x. In this paper, we found that the empirical selection of $c_1 = 1.4$ and $c_2 = 3.2$ is able to guarantee the accuracy of (18) up to an order of 50.

After specifying the points p and q, multipole expansion number P and sampling number Q, we can discuss the relationship between the order of Hankel functions and the minimum group size. As shown in Fig. 4, higher order of Hankel function requires larger group size to reduce the relative error. Therefore, the group size can not be too small in order to meet a specific error criteria. This fact has been defined as the low frequency break down problem for the zero-order

Hankel function [25]. For traditional FMM, this problem is not so critical since only zero-order Hankel function is involved and the group size can be as small as half wavelength. However, from Fig. 4, it can be seen that an overly small group will introduce greater calculation errors for higher-order Hankel functions which is the case often encountered in scattering matrix method.

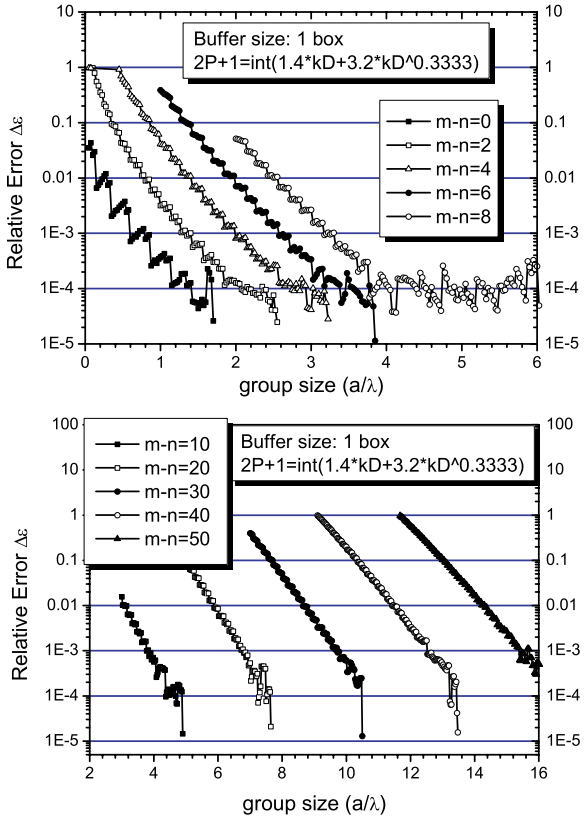

Figure 4. Relative error versus the group size for various order of Hankel functions.

From Fig. 4, we can get the minimum group size required for a specific order of Hankel function when the relative error is set to be 0.01 and 0.001 as shown in Fig. 5. In our code implementation, an empirical rule to determine the minimum group size a/λ versus order

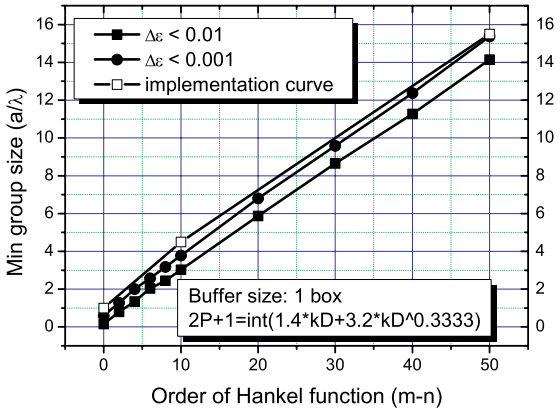

Figure 5. The relationship among minimum group size, order of Hankel functions and the accuracy required for 1 box buffer implementation.

of Hankel functions involved $m-n$ is given as following segment lines

$$\frac{a}{\lambda} = \begin{cases} 1.0 + 0.35(m-n) & m-n \leq 10 \\ 4.5 + 0.275(m-n) & 10 < m-n \leq 50 \end{cases} \tag{28}$$

Hence, in order to get accurate results, FMA-SMM first needs to know the maximum dimension of the T-matrix of involved cylinders. Then, a hierarchical group structure is set up from bottom up following the minimum group size given in (28). This procedure is different from that of the traditional FMM for integral equations. Once the group structure is set up, the near or far group set for each group are obtained steadily, and the sparse matrices in (22) can be calculated and stored in certain sparse matrix format. Iterative solvers are required to get the solution of (22). In this work, BiCGStab(2) are employed [24].

5. NUMERICAL RESULTS

First, the conventional SMM code is validated by comparing with previous publications. The accuracy and efficiency of FMA-SMM will be tested by comparing with the validated SMM code.

Figure 6 shows the scattering from two dielectric rods computed by our SMM code. Up to 25 cylindrical harmonics are used in T-matrix of each rod. Our results exactly meet those of Fig. 6 in [26]. Similar comparisons have been conducted with those in [27] and [28]. very good agreements are also found (not presented here due to limited pages).

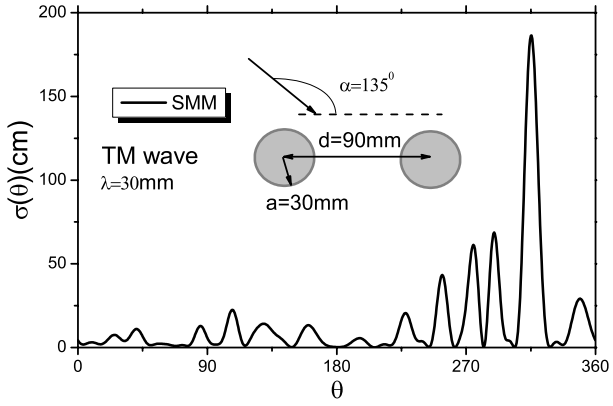

Figure 6. Bistatic scattering width of two dielectric rods ($\varepsilon_r = 2 : 25$).

To further test the near field calculation of the SMM code, a finite size photonic crystal structure with one defect proposed by Fig. 4 in [8] is analyzed. Fig. 7(a) compares present transmission spectra with that of [8]. A good agreement is found between these two results except for wavelengths with transmission below -35 dB. More importantly, the resonant wavelength is predicted to be $\lambda = 9.0572$, exactly same to that calculated in [8]. Fig. 7(b) shows the electric field distribution of the resonant mode, quite similar to the mode pattern shown in Fig. 6 of [8]. These numerical examples have verified our implementation of SMM code.

Figure 8(a) shows the electric field distribution of a photonic crystal power splitter proposed in [29] at $\lambda = 1.55\,\mu$m, a useful wavelength for current telecommunication systems. The whole structure is constructed by removing some rows or columns from a square lattice of infinitely long dielectric cylinders, whose pitch is $a = 0.4 \times 1.55 = 0.62\,\mu$m and the permittivity is $\epsilon_r = 11.56$. The black spots in Fig. 8(a) represent the position of total 465 dielectric rods. The radius of the rods is $0.18a = 0.11\,\mu$m. In our calculation, 3 harmonics are used for each rod. Therefore, there are 1395 unknowns in total. It can be seen that the agreements among FMA-SMM and SMM are quite good (refer to [29] for the field distribution which is obtained by FDTD). The figure shows that the power of electromagnetic wave is equally divided and transferred from one photonic crystal waveguide into two channels. Fig. 8(b) gives the residual errors versus iterative steps of BiCGStab [24] for both FMA-SMM and SMM. The convergence rate of FMA-SMM is almost equal to the conventional SMM. It takes a total of 158 seconds for SMM to fill

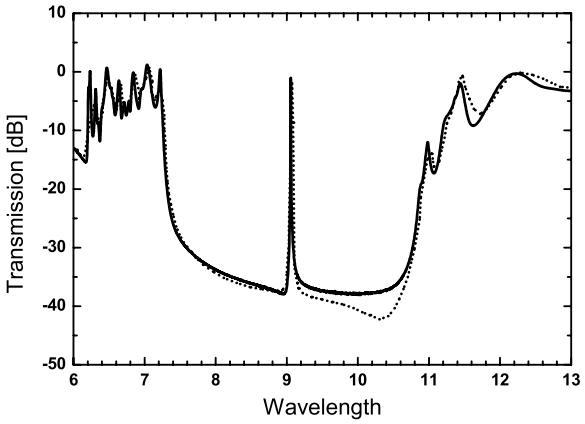

(a)

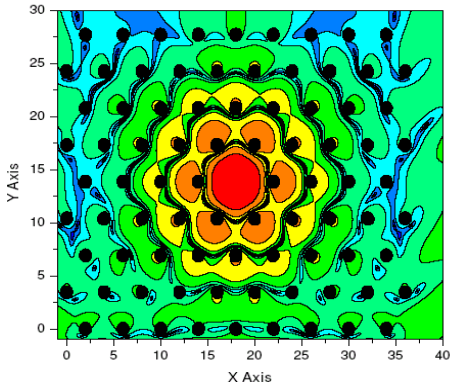

(b)

Figure 7. (a) Transmission spectra of a finite size photonic crystal with one defect (solid line: present; Dash line: [8]), (b) Electric field distribution of the resonant mode ($\lambda = 9 : 0572$).

up all the matrix elements and get the final solution while FMA-SMM only uses 72 seconds, nearly two times faster than SMM.

Furthermore, a triangular lattice of cylindrical rods as shown in Fig. 9 is used to test the accuracy and efficiency of the FMA-SMM algorithm. It is assumed that there are M_x column and M_y row circular dielectric rods with radius r_0. (In this figure, $M_x = 9$, $M_y = 11$). The period of these rods is a and $b/2$ in x and y directions, respectively.

Figure 10 compares the FMA-SMM and SMM results for scattering patterns of a triangular lattice of metal rods. It can be seen that the maximum absolute errors of these two methods are less than

0.3 dB. Such good agreements of FMA-SMM and SMM demonstrated in Fig. 8 and Fig. 10 have verified the accuracy of FMA-SMM for both near and far fields computing.

To obtain the computational complexity of FMA-SMM in terms of CPU time and memory cost, different size problems are simulated by varying the row number M_y of the triangular lattice of rod array shown in Fig. 9 while keeping the column number of rods constant. In the following examples, we select $M_x = 20$ and row number M_y is chosen from 20 to 110. The radii and dielectric constant of all the rods are set as $r_0 = 0.2\lambda$, $\varepsilon_r = 3.0$. TM wave illumination is assumed and seven harmonics are used for each dielectric rod.

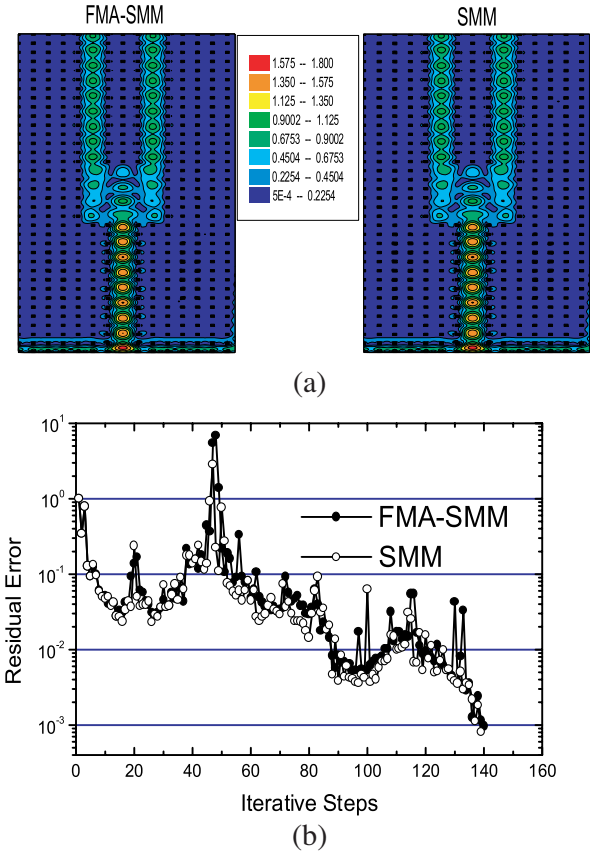

Figure 8. (a) Electric field distribution of a multimode interference-based photonic crystal power splitter, (b) iterative procedure of FMA-SMM and SMM.

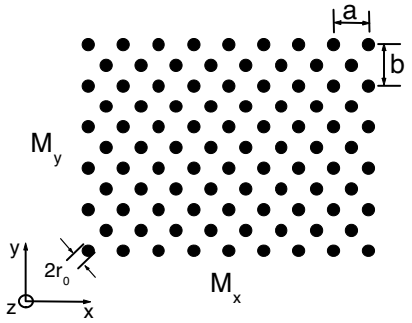

Figure 9. Schematic of triangular lattice of cylindrical rods.

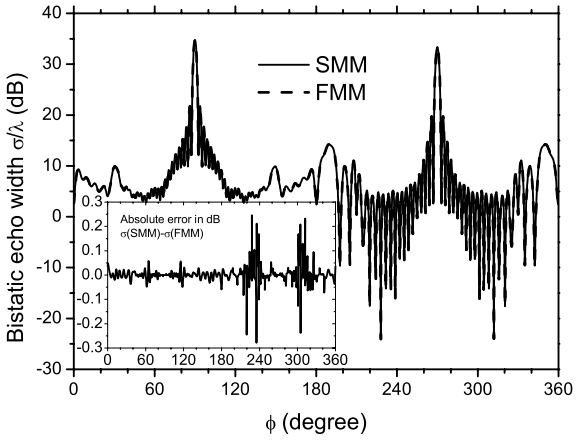

Figure 10. Comparison of SMM and FMA-SMM for bistatic echo width of a rod array ($a = 1.0\lambda$, $b = 2.0\lambda$, $M_x = 21$, $M_y = 10$, $r_0 = 0.4\lambda$, $\phi^{inc} = 90°$, total 205 metal rods in case of TM incidence.

Moreover, in order to investigate the impact of rod density on the computational complexity and convergence properties of the algorithm, two specific cases with different lattice spacings are carefully studied

- **case 1:** $a = 0.5\lambda$, $b = 1.0\lambda$.
- **case 2:** $a = 1.0\lambda$, $b = 2.0\lambda$.

Figure 11 shows the comparison of SMM and FMA-SMM on memory cost versus unknowns. Obviously, the density of rods does not influence the memory cost of SMM. However, for FMA-SMM, case 1 requires more memory than case 2. This is because case 1

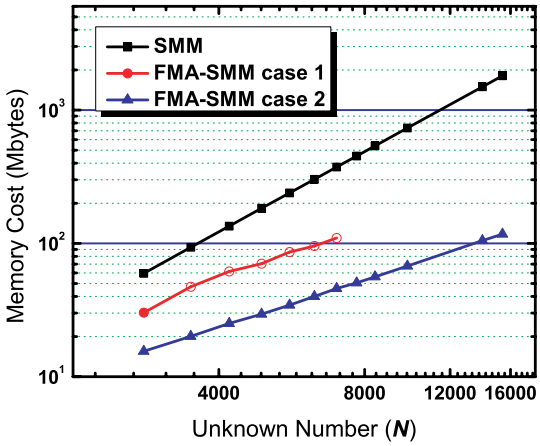

Figure 11. Memory requirement comparison of SMM (estimated) and FMA-SMM for different density of cylinders.

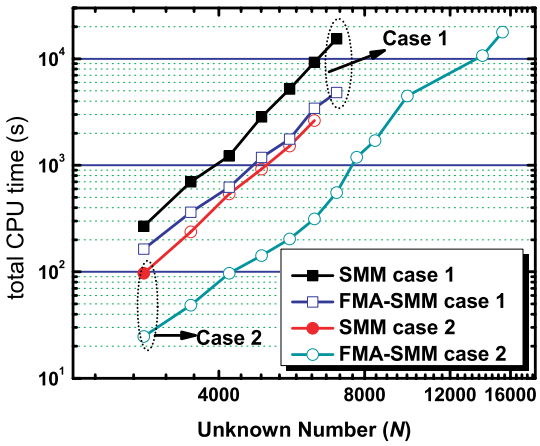

Figure 12. Total CPU time versus unknowns of SMM and FMA-SMM for different cases.

has higher rod density and thus, results more elements stored in near group interaction matrix $\mathbf{S}_N$ in (22).

Figure 12 provides the total CPU time versus unknowns for SMM and FMA-SMM in both case 1 and 2. It can be seen that in both cases, FMA-SMM is faster than SMM. On the other hand, for case 1, both SMM and FMA-SMM requires much more CPU time than their counterparts in case 2. This can be explained by Fig. 13. More

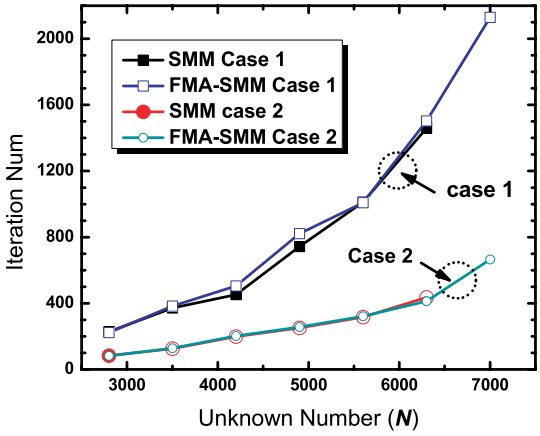

Figure 13. Comparison of iteration numbers versus unknowns solving with SMM and FMA-SMM using BiCGStab(2).

iterative steps are needed for denser rod lattice due to stronger mutual scattering than those in sparser one. The residual error criteria is set to be 0.001 for BiCGSTab(2) in all numerical results in this paper. Fig. 13 shows that SMM and FMA-SMM needs almost same iteration numbers to converge. This indicates the equation matrix in FMA-SMM formula (22) has almost same condition number to the matrix in (5). This, from another aspect, verifies the effectiveness of FMA-SMM.

For case 1, BiCGStab(2) fails to converge to the relative error criteria for the lattice with more than 1000 cylinders. That's the reason no memory cost and CPU time data are given when unknown number is more than 7000 for case 1 in Figs. 11 and 12. For analysis of a large number of dense rods, more efficient iterative solver needs to be further studied.

Finally, to demonstrate the powerfulness of the FMA-SMM algorithm, the bistatic scattering pattern of the largest array we simulated in case 2 is shown in Fig. 14. The array contains 2200 rods ($M_y = 110$) and occupies more than $2,200\lambda^2$ area. Then the total unknown N is 15,400. Fig. 15 shows the iterative history of BiCGStab(2) for simulation of 14. It takes total 5752 iterative steps and 17,758 seconds (nearly 5 hours) to reach the residual error 8.94114×10^{-4}. Traditional scattering matrix method requires more than 1.8 Gbytes memory while the new algorithm developed needs less than 0.12 Gbytes memory. In this case, the novel FMA-SMM is nearly 15 times faster than conventional SMM. This example demonstrates that FMA-SMM can dramatically reduce the memory cost of SMM.

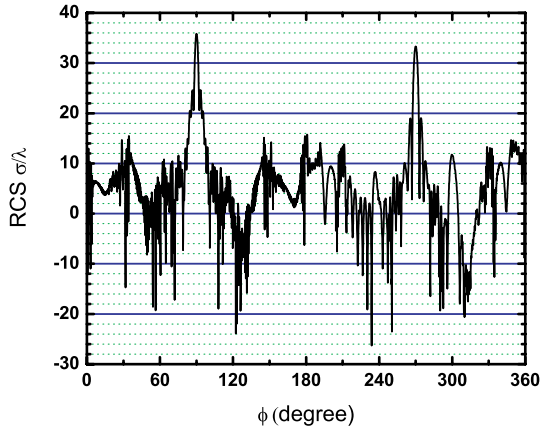

Figure 14. Bistatic scattering from a large array of 2200 dielectric rods ($a = 1.0\lambda$, $b = 2.0\lambda$, $M_x = 20$, $M_y = 110$, $r_0 = 0.2\lambda$, $\epsilon_r = 3.0$, $\phi^{inc} = 90°$).

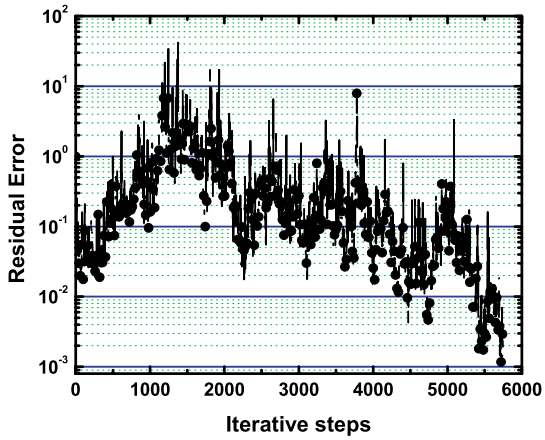

Figure 15. Iterative history of BiCGStab(2) for FMA-SMM solution of Fig. 14.

However, the convergence rate remains same to SMM, quite slow for dense lattice or lattice with a large number of rods. How to construct efficient preconditioning technique is critical for FMA-SMM's further applications.

The above examples demonstrate the potential applications of the novel FMA-SMM in many applications, for example, in analysis of photonic crystal devices.

6. CONCLUSION

The general fast multipole expressions of arbitrary order Hankel functions are derived by using lowering and raising operators. An efficient algorithm, fast multipole accelerated scattering matrix method (FMA-SMM), is proposed for analysis of multiple scattering from a large number of cylinders. The empirical formula is provided to determine the minimum group size in FMA-SMM versus the highest order of Hankel functions involved. The accuracy of the algorithm is validated by comparing with previous studies of both near field distribution and the far field radiation pattern. Numerical examples demonstrate the lower computational complexity in memory requirements and CPU time of the novel fast algorithm. An example of a large array with more than two thousands cylinders is provided to show the efficiency of the FMA-SMM. The novel fast algorithm can be used in simulation of various 2D photonic crystal devices.

REFERENCES

1. Foldy, L. L., "The multiple scattering of waves I. General theory of isotropic scattering by randomly distributed scatterers," *Phys. Rev.*, Vol. 67, 107–119, Feb. 1945.
2. Lax, M., "Multiple scattering of waves," *Rev. Mod. Phys.*, Vol. 23, 287–310, Oct. 1951.
3. Twersky, V., "Multiple scattering of radiation by an arbitrary configuration of parallel cylinders," *J. Acoust. Soc. Am*, Vol. 24, 42–46, Jan. 1952.
4. Waterman, P. C., "New formulation of acoustic scattering," *J. Acoust. Soc. Am.*, Vol. 45, 1417–1429, June 1969.
5. Waterman, P. C., "Symmetry, unitarity, and geometry in electromagnetic scattering," *Phys. Rev. D*, Vol. 3, 825–829, Feb. 1971.
6. Peterson, B. and S. Ström, "T-matrix for electromagnetic scattering from an arbitrary number of scatterers and representation of E(3)," *Phys. Rev. D*, Vol. 8, 3661–3678, Nov. 1973.
7. Chew, W. C., C. C. Lu, and Y. M. Wang, "Efficient computation of three-dimensional scattering of vector electromagnetic waves," *J. Opt. Soc. Am. A*, Vol. 11, 1528–1537, Apr. 1994.
8. Tayeb, G. and D. Maystre, "Rigorous theoretical study of finite-size two-dimensional photonic crystals doped by microcavities," *J. Opt. Soc. Am. A*, Vol. 14, 3323–3332, Dec. 1997.

9. Yonekura, J., M. Ikeda, and T. Baba, "Analysis of finite 2-D photonic crystals of columns and lightwave devices using the scattering matrix method," *J. Lightwave Tech.*, Vol. 17, 1500–1508, Aug. 1999.
10. Li, E. P., Q. X. Wang, Y. J. Zhang, and B. L. Ooi, "Analysis of finite-size coated electromagnetic bandgap structure by an efficient scattering matrix method," *IEEE J. Selected Topics Quantum Elect.*, Vol. 11, 485–492, Mar.–Apr. 2005.
11. Kuo, C.-H. and Z. Ye, "Negative-refraction like behavior revealed by arrays of dielectric cylinders," *Phys. Rev. E*, Vol. 70, 026608, 2004.
12. Shooshtari, A. and A. R. Sebak, "Electromagnetic scattering by parallel metamaterial cylinders," *Progress In Electromagnetics Research*, PIER 57, 165–177, 2006.
13. Boscolo, S. and M. Midrio, "Three-dimensional multiple-scattering technique for the analysis of photonic-crystal slabs," *J. Lightwave Tech.*, Vol. 22, 2778–2786, Dec. 2004.
14. Talebi N., M. Shahabadi, and C. Hafner, "Analysis of a lossy microring using the generalized multipole technique," *Progress In Electromagnetics Research*, PIER 66, 287–299, 2006.
15. Koc, S. and W. C. Chew, "Calculation of acoustical scattering from a cluster of scatterers," *J. Acoust. Soc. Am*, Vol. 103, 721–734, Feb. 1998.
16. Gumerov, N. A. and R. Duraiswami, "Computation of scattering from clusters of spheres using the fast multipole method," *J. Acoust. Soc. Am*, Vol. 117, 1744–1761, Apr. 2005.
17. Cheng, H., W. Y. Crutchfield, Z. Gimbutas, L. F. Greengard, J. F. Ethridge, J. Huang, V. Rokhlin, N. Yarvin, and J. Zhao, "A wideband fast multipole method for the Helmholtz equation in three dimensions," *J. Comput. Phys.*, Vol. 216, 300–325, July 2006.
18. Gumerov, N. A. and R. Duraiswami, *Fast Multipol Methods for the Helmholtz Equation in Three Dimensions*, Elsevier Ltd., 2004.
19. Rokhlin, V., "Rapid solution of integral equations of scattering theory in two dimensions," *J. Comput. Phys.*, Vol. 86, 414–439, Feb. 1990.
20. Engheta, N., W. D. Murphy, V. Rokhlin, and M. S. Vassiliou, "The fast multipole method (FMM) for electomagnetic scattering problems," *IEEE Trans. Antennas Propagat.*, Vol. 40, 634–641, June 1992.
21. Lu, C. C. and W. C. Chew, "Fast algorithm for solving hybrid

integral equations," *IEE Proc.-H*, Vol. 140, 455–460, Dec. 1993.

22. Chew, W. C., J. M. Jin, E. Michielssen, and J. M. Song, *Fast and Efficient Algorithms in Computational Electromagnetics*, Artech House, 2001.
23. Chew, W. C., *Waves and Fields in Inhomogeneous Media*, Van Nostrand Reinhold, New York, U.S.A, 1990.
24. Van der Vorst, H. A., "Bi-CGSTAB: A fast and smoothly converging variant of Bi-CG for the solution of non-symmetric linear systems," *SIAM J. Sci. Stat. Comput.*, Vol. 13, 631–644, 1992. (BiCGStab code available at http://www.math.uu.nl/people/vorst/ zbcg2.f90)
25. Ohnuki, S. and W. C. Chew, "Numerical accuracy of multipole expansion for 2-D MLFMA," *IEEE Trans. Antennas Propagat.*, Vol. 51, 1883–1890, Aug. 2003.
26. Felbacq, D., G. Tayeb, and D. Maystre, "Scattering by a random set of parallel cylinders," *J. Opt. Soc. Am. A*, Vol. 11, 2526–2538, Sep. 1994.
27. Elsherbeni, A. Z. and M. Hamid, "Scattering by parallel conducting circular cylinders," *IEEE Trans. Antennas Propagat.*, Vol. AP-35, 355–358, Mar. 1987.
28. Ragheb, H. A. and M. Hamid, "Simulation of a cylindrical reflector by conducting circular cylinders," *IEEE Trans. Antennas Propagat.*, Vol. AP-35, 349–353, Mar. 1987.
29. Liu, T., A. R. Zakharian, M. Fallahi, V. Moloney, and M. Mansuripur, "Multimode Interference-based photonic crystal waveguide power splitter," *J. Lightwave Tech.*, Vol. 22, 2842–2846, Dec. 2004.